



# Interface reaction during titanium alloys investment casting by residue gas in ceramic mold

Ya-Meng Wei , Zhi-Gang Lu\* , Xin-Yi Li, Xin Guo

Received: 1 April 2018 / Revised: 29 May 2018 / Accepted: 9 August 2018 / Published online: 11 October 2018  
© The Nonferrous Metals Society of China and Springer-Verlag GmbH Germany, part of Springer Nature 2018

**Abstract** The chemical reaction between mold material and titanium melt during investment casting was studied intensively. However, the influence of residue gas in ceramic mold on interface reaction remains unclear. In this investigation, the effect of residue gas in  $Y_2O_3$ -silica sol shell mold on interface reaction during Ti-6Al-4V alloy investment casting was investigated. Two groups of shell molds were prepared by adding different kinds of pore formers, i.e., spherical starch particles or nylon fibers, respectively. Ti-6Al-4V alloy was cast under vacuum by gravity casting through cold crucible induction melting (CCIM) method. Porosity of different shell molds was measured based on Archimedeian method. Scanning electron microscopy (SEM) and energy-dispersive X-ray spectroscopy (EDS) were employed to characterize the micromorphology and composition of the reaction area, respectively. White light interferometer (WLI) was used to obtain the surface topography of the shell mold. The results show that the direct chemical reaction is very weak for all specimens. The release of residue gas in closed pores is the key factor influencing surface defects. However, open pores make nearly no difference on the interface reaction.

**Keywords** Titanium alloy; Investment casting; Residue gas;  $Y_2O_3$ ; Silica sol

## 1 Introduction

The utilization of titanium alloy is continuously increasing in aviation because it can reduce the weight of aircraft markedly [1]. Investment casting is one of the most efficient and economical manufacturing methods for the near-net formation of complex titanium alloy parts [2]. However, titanium melt will react with almost all the mold materials because of the high chemical activity, which badly affects the quality of castings [3–6]. The chemical inertness against titanium melt of common refractory materials such as  $ZrO_2$  [7, 8], CaO [9, 10],  $Al_2O_3$  [11], NiCrAlY [12] and  $Y_2O_3$  [13–16] has been studied extensively based on Gibbs free energy ( $\Delta G_f$ ) analysis. The results of these studies showed that  $Y_2O_3$  might be the best choice as a shell mold material due to its excellent inertness against titanium alloy melt. Tetsui et al. [17] and Zhao et al. [18] conducted systematic pouring experiments using different refractory materials, respectively, and found the least oxygen enrichment in titanium parts when  $Y_2O_3$  primary layer was employed. Wei et al. [19] proved that Ti-6Al-4V castings with almost none reaction layer could be obtained using  $Y_2O_3$ -silica sol mold. Based on previous studies [19–22], titanium castings with very thin reaction layer could be obtained when cast in high inert shell mold under proper process conditions.

However, the aforementioned studies are mainly focused on the direct chemical reaction and interface contamination layer, whereas studies on the effect of environmental factors are still lacking. The environmental

Y.-M. Wei, Z.-G. Lu\*, X.-Y. Li  
Department of Mechanical Engineering, Tsinghua University,  
Beijing 100084, China  
e-mail: lvzg@mail.tsinghua.edu.cn

Y.-M. Wei, Z.-G. Lu, X.-Y. Li  
State Key Laboratory of Tribology, Tsinghua University,  
Beijing 100084, China

X. Guo  
Academy of Opto-Electronics, Chinese Academy of Sciences,  
Beijing 100094, China

factors may also lead to surface defects and deteriorate the surface quality. Guo et al. [23] conducted the pouring experiment under working conditions and confirmed that the residue gas in the environment during pouring had critical influence on surface quality of casting product. Campbell [24] and Srivastava et al. [25] found that the surface of titanium melt could be easily oxidized by environmental gas and the entrained oxide films in titanium alloys were pretty common. In the actual production of titanium products, the contamination layer can be eliminated through pickling and sand blasting process. However, the other surface defects, such as surface pores and non-metallic inclusions, are even more difficult to be eliminated, resulting in the rejection of castings. The ceramic mold is a kind of porous material. Because of the inhomogeneity of stucco and drying processing [26], some parts of the shell mold contain more residue gas than average. A portion of the residues gas is sealed in closed pores and cannot be expelled even under vacuum which may involve in the interface reaction during the pouring process. But up to now, there are few reports on the effect of residue gas in ceramic mold on interface defects.

The aim of this study is to clarify the effect of residue gas in ceramic mold on interface defects. Two groups of shell molds were prepared by adding different kinds of pore formers, i.e., spherical starch particles or nylon fibers, and Ti-6Al-4V alloy was poured into these shell molds. The reaction mechanism between titanium and the residue gas in ceramic mold was also studied.

## 2 Experimental

First, silica sol and  $Y_2O_3$  filler were mixed and fully stirred to make the primary layer slurry. The slurry was averagely divided into three beakers. The microstructure of pore formers used in this investigation is shown in Fig. 1, and they were added to two beakers, respectively. The other one was applied as a control group. The adding amount of

pore former was 2 wt% of the slurry. The final primary layer slurries used in experiment were prepared after fully stirring again. The back-layer slurries were made of silica sol and mullite fillers using the similar method. Each shell sample contained two primary layers and four back layers, and the shell specifications are summarized in Table 1.

Figure 2a shows the design of wax pattern in which twelve  $20\text{ mm} \times 20\text{ mm} \times 6\text{ mm}$  cuboids adhere to a cylinder gate. The cuboids were coated with the prepared slurries according to Table 1 through brush-painting method and stuccoed with refractory materials, thereby forming the ceramic mold.  $Y_2O_3$  sand and mullite sand were chosen as refractory material for primary layer and back layer, respectively. The drying time between layers was 12 h. Figure 2b shows the ceramic shell mold after steam dewaxing. Finally, the shell was fired in a type furnace in air with a heating rate of  $10\text{ }^\circ\text{C}\cdot\text{min}^{-1}$  to  $1050\text{ }^\circ\text{C}$  and held for 12 h before pouring.

The cold crucible induction melting (CCIM) method was employed in a furnace ZG-2XF that consisted of a crucible, which can hold 2 kg pure titanium. The melting of Ti-6Al-4V alloy was conducted under a pressure of  $2 \times 10^{-2}\text{ Pa}$ , and the pouring temperature of the melt was around  $1700\text{ }^\circ\text{C}$ . The ceramic shell was preheated to about  $200\text{ }^\circ\text{C}$  before pouring.

The  $20\text{ mm} \times 20\text{ mm} \times 6\text{ mm}$  titanium alloy samples for further analysis were cut at the middle in the direction parallel to the cylinder gate by wire electrical discharge machining (WEDM) and then subjected to finishing processes of grinding and polishing. Scanning electron microscope (SEM, MERLIN VP Compact, Carl Zeiss, Jena, Germany) equipped with energy-dispersive X-ray spectroscope (EDS) was used to characterize the structure and composition of the reaction layer of the castings. X-ray photoelectron spectroscope (XPS, Hammer's, 250XI, UK) was utilized to confirm the valence state of relevant elements, and white light interferometer (WLI, Veeco, Dektak 150, USA) was applied to obtain the surface profile of the shell molds. The porosities of different ceramic molds were

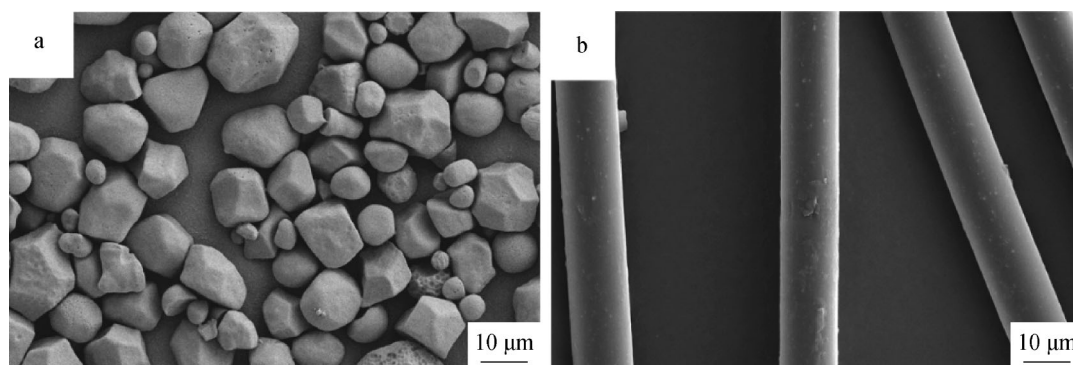


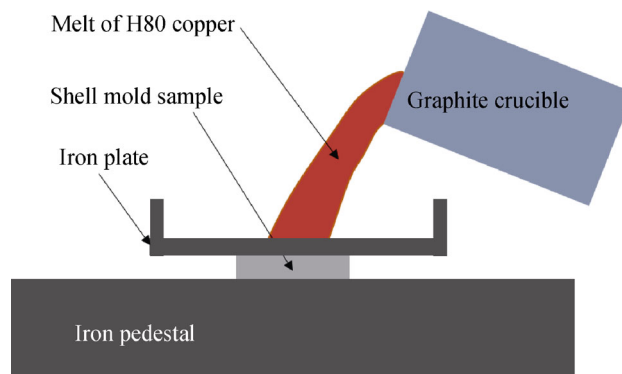
**Fig. 1** SEM images of **a** starch pore former and **b** nylon fiber pore former

**Table 1** Shell mold specifications for pouring experiment

Samples	Primary layer		Back layer			
	First	Second	First	Second	Third	Fourth
S0	Normal		Normal			
S1	Starch		Normal			
S2	Normal		Starch			
S3	Starch		Starch		Normal	Normal
F1	Fiber		Normal			
F2	Normal		Fiber			
F3	Fiber		Fiber			

tested according to GB/T 25995-2010 which was based on Archimedes principle. The size of shell molds for porosity test was 40 mm × 20 mm × 3 mm. The porosities of pure primary shell, 2 wt% starch containing primary shell, 2 wt% nylon containing primary shell, pure back shell, 2 wt% starch containing back shell and 2 wt% nylon containing back shell were tested in this paper. They were labeled as pure primary shell (PP), 2 wt% starch containing primary shell (PS), 2 wt% nylon containing primary shell (PF), pure back shell (BP), 2 wt% starch containing back shell (BS) and 2 wt% nylon containing back shell (BF), respectively.

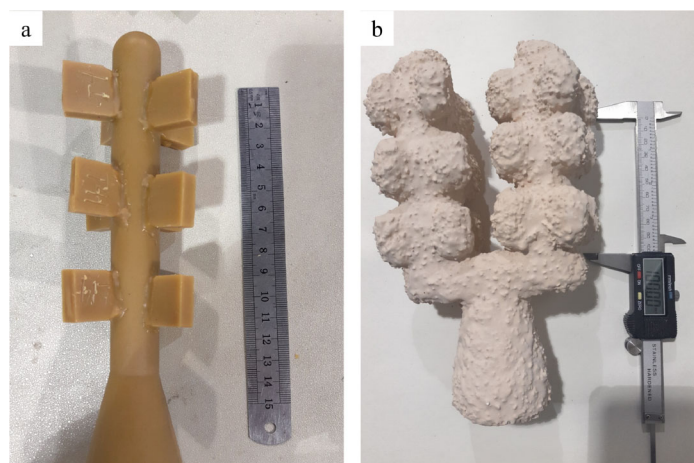
Shell thermal shock experiment was conducted to simulate the behavior of shell mold during the pouring process. Ceramic shell mold sample was covered by a thin iron plate made of 304 stainless steel shown in Fig. 3. Two hundred grams of H80 copper melt at 1100 °C was poured in the steel plate. After cooling to room temperature, the sample after thermal shock was observed through optical microscope (OM, Zeiss, Axio Lab A1, Germany).

**Fig. 3** Design of thermal shock experiment

### 3 Results and discussion

#### 3.1 Structure and composition of interface reaction layer

Generally, S1, S2, S3, F1, F2 and F3 samples have smooth surfaces and metallic luster through visual observation. The cross section of the pore former containing samples was examined by SEM and EDS, as shown in Fig. 4. EDS line scanning shows that the distribution of Ti, O, Y and Si in S1, S2, S3, F1, F2 and F3 samples is homogeneous and almost does not change with the depth from the surface to the interior of the samples, meaning that the direct chemical reaction between titanium melt and ceramic mold is very mild. The thickness of reaction layer is limited to several micrometers indicated by the distribution of O and Si. The similar phenomenon was also observed in the previous work [19] using  $Y_2O_3$ -silica sol primary shell mold. The addition of pore former, whether it is starch or fiber, does not seem to influence the direct reaction degree. When it comes to the micromorphology, the difference is obvious. S1, S2, S3 and F2 samples have a fluctuant

**Fig. 2** Design of **a** wax pattern and **b** shell mold after steam dewaxing

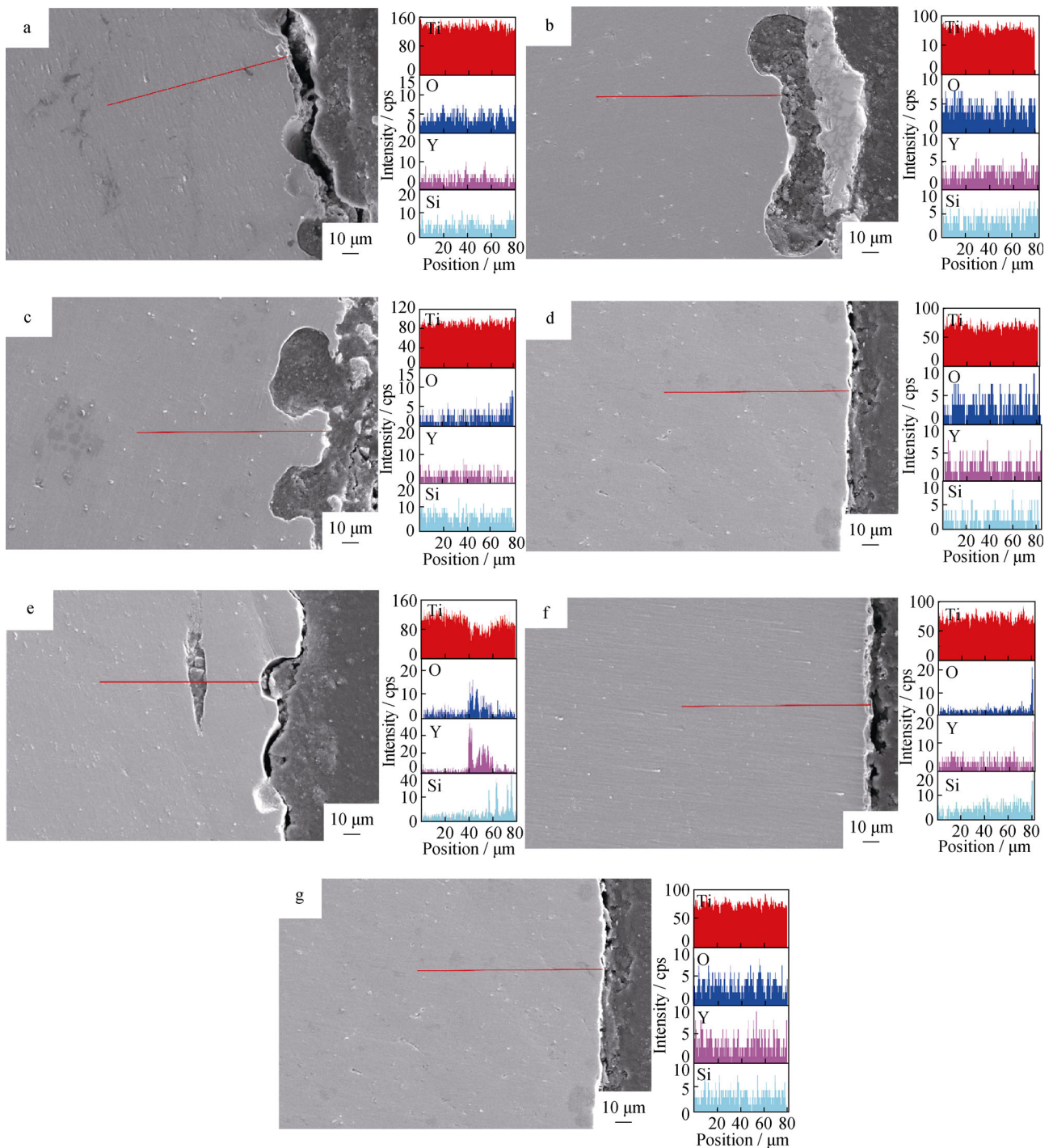


**Fig. 4** Cross-sectional SEM images and line-scan EDS analysis of **a** S1, **b** S2, **c** S3, **d** F1, **e** F2, **f** F3 and **g** S0 samples

interface with obvious pores at the surface of the casting, while the cross-sectional boundary of F1 and F3 samples is flat and almost the same with that of S0 sample. Except for the surface pores mentioned above, inclusions are also scattered near the surface, as shown in Fig. 4e. The discontinuous peaks of O, Y and Si in Fig. 4e indicate that it is inclusion rather than diffusion.

To better understand the forming mechanism of the surface pores, more detailed analysis was made on a typical surface pore found in S3 sample, as shown in Fig. 5. The surface pore presents a typical morphology of intrusive blowhole. Obvious Si and O are observed in the inner wall of the pore, as shown by EDS map scanning, indicating that the gas comes from inside the shell mold. Besides, slight



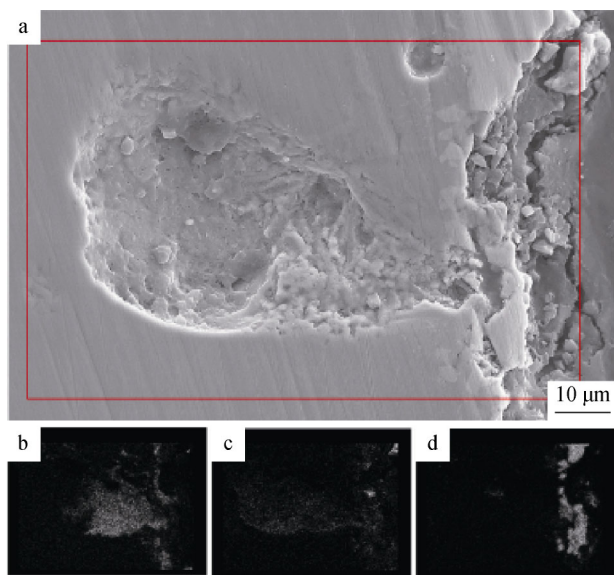


**Fig. 5** SEM image for a typical surface pore found in S3 sample and EDS map scanning of **b** Si, **c** O and **d** Y

chemical scabs are found near the pore according to the distribution of Y. These pores would become punctate defects during fluorescence detection and could not be eliminated easily through pickling and sandblasting because they are too deep to be cleared. They are more severe than traditional contamination layer in one way as the latter can be removed through sandblasting.

It could not be ignored that not all pores stay at the surface and some of them go inside the metal and become internal blowholes. Most of these internal pores have a long tail. Figure 6 shows microstructure of a typical pore found in F2 sample. The right side of Fig. 6 shows the internal pore and its tail. To obtain a quantitative elemental distribution in the tail, a series of EDS spot scanning was conducted as the yellow square shows. Si content in the tail is obvious larger than in the adjacent region. The experimental phenomena mentioned above will be explained in the following section.

### 3.2 Structure analysis of shell mold

The porosities of pure primary shell (PP), 2 wt% starch containing primary shell (PS), 2 wt% nylon containing primary shell (PF), pure back shell (BP), 2 wt% starch containing back shell (BS) and 2 wt% nylon containing back shell (BF) were tested and are shown in Table 2. Pure primary shell mold has a true porosity around 30%, and pure back layer shell mold has a true porosity around 25%. The addition of 2 wt% pore former, no matter starch or fiber, increases the total porosity by around 5.7% for primary shell mold and 4.6% for back shell mold. It is because that the sintering degree of  $Y_2O_3$ -silica sol primary shell

mold and Al-Si back shell mold is different. The former has only very limited solid- and liquid-state sintering, while the latter has obvious liquid-state sintering which leads to a denser structure and decreases the porosity. As shown in Table 2, the type of pore former does not influence the total amount of porosity notably; however, it changes the type of pores. The addition of starch brings 150% more closed porosity in primary shell and 53% more closed porosity in back shell, while the addition of nylon fiber is not as efficient in increasing closed porosity in ceramic shell mold. The main reason is that the starch is nearly spherical and nylon is fibrous. After sintering, nylon was burnt out and many air passages were formed, which brings larger apparent porosity.

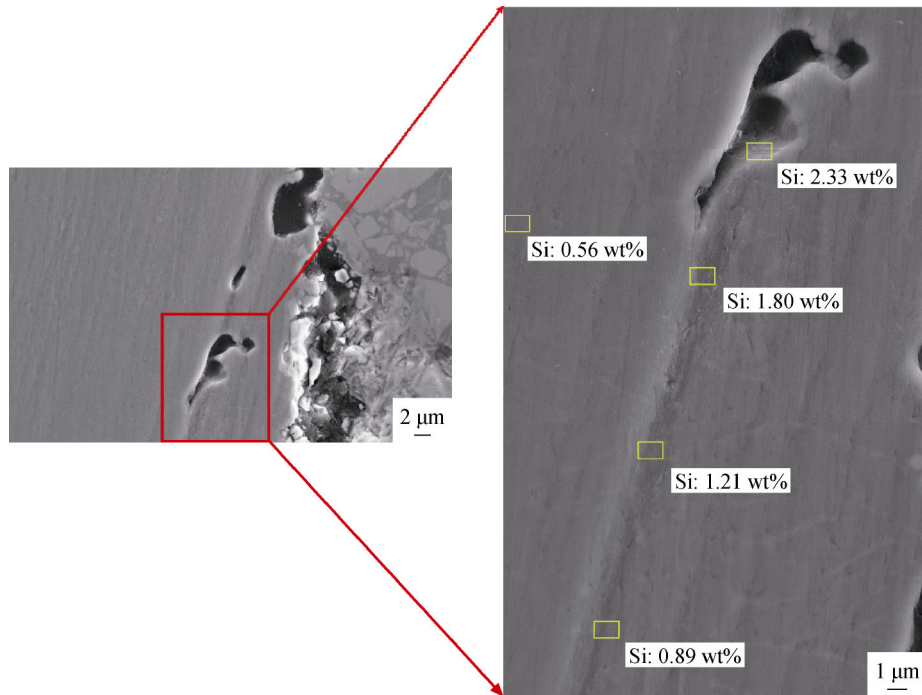
Except for the porosity, the microstructure of different shell molds was also studied. The surface profiles of shell molds were obtained by WLI, and the results are shown in Fig. 7. The surface morphology undulation of shell PS and PF is more severe than that of PP because of the surface pores formed by pore former. The surface roughness of shell mold increases from 20% to 30% due to the surface pores as shown by the dark blue points in Fig. 6b, c.

Figure 8 shows microphotographs of the shell mold obtained by SEM. As for PP, the surfaces were flat. As for pore-former-added sample, PS had some pores as shown in Fig. 8b and we can see the bottom of these pores clearly, while for PF, pores were also found on the surface; however, it extended to the interior of the ceramic mold. When it came to BP, BS and BF, the differences were not as large. None obvious surface pores could be found in BS and BF as a result of the densification process during the sintering.

The schematic diagram of pore distributions in different shells was drawn based on analyses above and is shown in Fig. 9. Sample PP had a certain amount of residue gas inside which cannot be expelled even in vacuum. The addition of starch particles increased the amount of residue gas in closed pores as shown in Fig. 8b, while the addition of fiber brings some gas way in the ceramic shell which increases the apparent porosity greatly rather than the closed porosity.

### 3.3 Physics simulations experiment

Shell thermal shock experiment was conducted to simulate the behavior of shell mold during pouring process. Melt of H80 copper at 1100 °C was poured on the plate shown in Fig. 3. After cooling down, the surface morphology of ceramic mold was observed by OM and is shown in Fig. 10. PS has severe cracks on the surface, and PF has relatively slight cracks. As for PP, its surface is still smooth and flat. It indicates that the addition of starch would promote the crack of shell mold during pouring process.



**Fig. 6** SEM image and corresponding enlarged image for a typical internal pore found in F2 sample

**Table 2** Porosity of different ceramic mold samples

Samples	True porosity/%	Apparent porosity/%	Closed porosity/%
PP	29.69	28.31	1.38
PS	35.30	31.86	3.45
PF	35.50	33.38	2.12
BP	25.06	21.94	3.12
BS	29.79	25.03	4.76
BF	29.49	25.70	3.78

### 3.4 Analysis on reaction mechanism

The structure of shell mold was studied. During the shell mold building process, some gas was sealed in the shell forming the closed pores. The gas could not be expelled in

the dewaxing process, roasting process and even under vacuum condition. This residue gas would have a centralized release when pouring. Based on the analysis of shell mold structure above, a shell structure schematic graph was built, as shown in Fig. 11. According to the shell mold structure and interface reaction analysis above, a reaction-release-entraining model was built. The surface defects forming process could be divided into three stages: the direct chemical reaction stage, the residue gas release stage and the entraining stage.

In the first stage, the titanium melt reacted directly with primary shell mold, forming a very thin reaction film (the orange film shown in Fig. 11). The thickness of this film was limited to several micrometers which was consistent with the previous study [19]. At almost the same time, the second stage began. When the high-temperature titanium

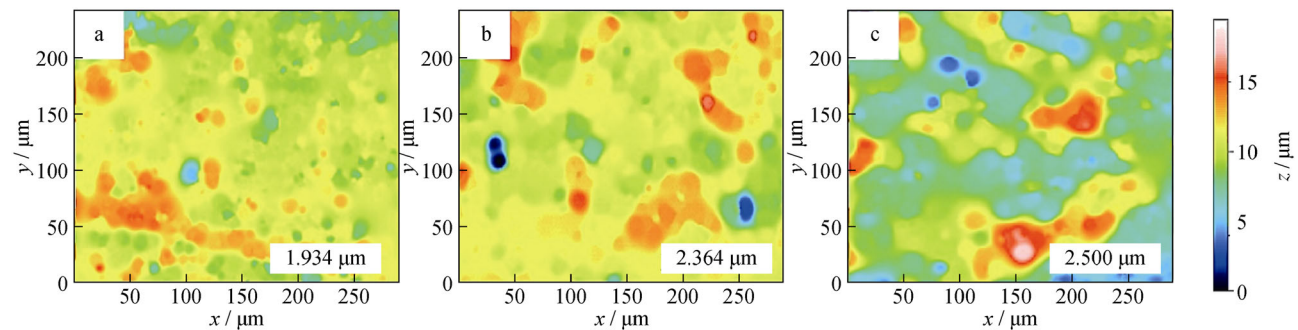


**Fig. 7** WLI images for surface microtopography of **a** PP, **b** PS and **c** PF

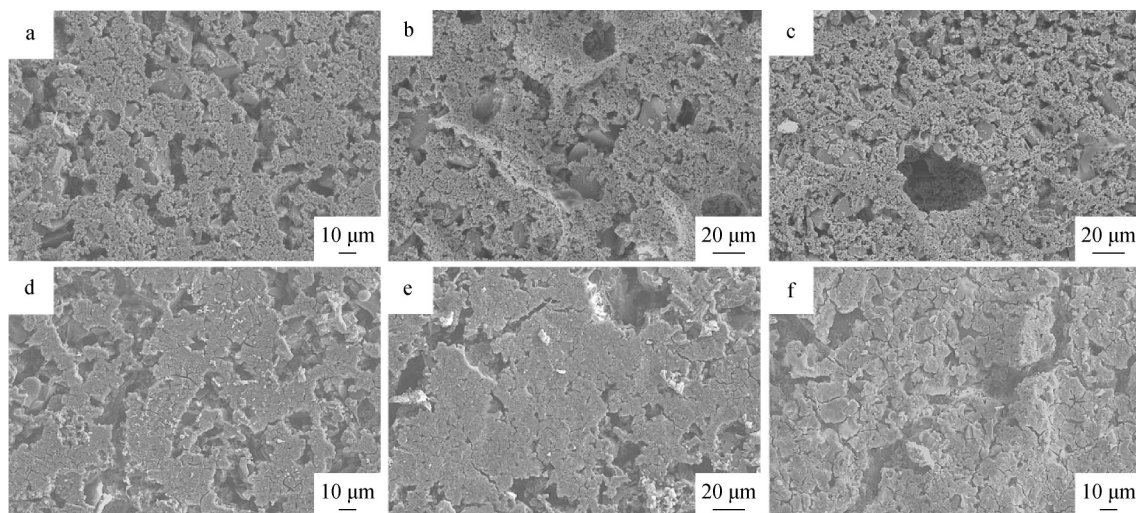


**Fig. 8** SEM images of **a** PP, **b** PS, **c** PF, **d** BP, **e** BS and **f** BF

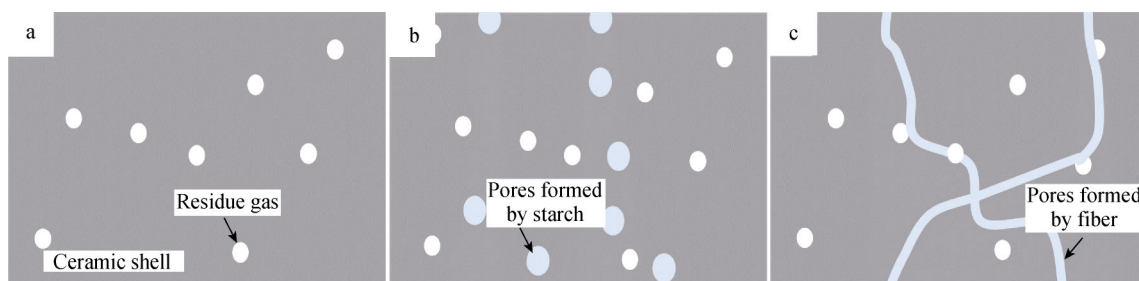


**Fig. 9** Schematic diagram showing pore distributions of **a** PP, **b** PS and **c** PF

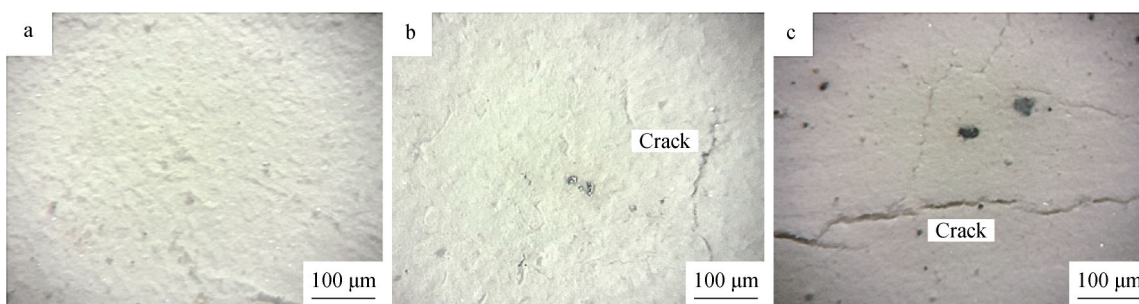


**Fig. 10** OM images for interface micromorphology of **a** S0, **b** S2 and **c** S3 samples

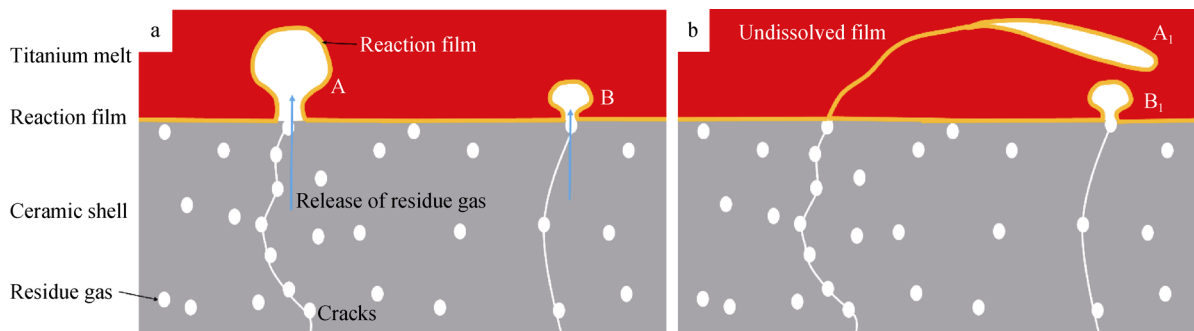


**Fig. 11** Schematic diagram showing reaction mechanism of residue gas in shell mold



melt contacted the shell mold, cracks in the shell mold appeared because of the thermal shock and increasing pressure in the closed pores. The residue gas would have a centralized release through these cracks at this time as Fig. 11a shows. The stress at gas release stage was caused by thermal shock and gas pressure in closed pores. The thermal stress can be calculated as Eq. (1) shows, and the stress from gas pressure can be calculated as Eq. (2) shows in which the closed pore was modeled as a tiny spherical pressure vessel.

$$\sigma_h = \frac{\alpha E}{1 - \mu} \Delta T \quad (1)$$

$$\sigma_p = \frac{pD}{4S} = \frac{3nRT}{4\pi D^3} \cdot \frac{D}{4S} = \frac{3nRT}{16\pi D^2} \quad (2)$$

where  $\sigma_h$  is thermal stress from thermal shock;  $\sigma_p$  is stress from gas pressure;  $\alpha$  is coefficient of linear expansion;  $E$  is elasticity modulus;  $\mu$  is Poisson's ratio;  $\Delta T$  is temperature difference;  $p$  is pressure in closed pore;  $D$  is radius of closed pore;  $S$  is the thickness of ceramic spherical;  $R$  is universal gas constant;  $T$  is the temperature;  $n$  is the amount of substance of gas.

The ceramic shell is a kind of brittle material, and the broken shell mold should follow the max tension stress criterion. When melt flows through the shell, both  $\Delta T$  and  $T$  near the mold surface increase shapely. As a result,  $\sigma_h$  and  $\sigma_p$  increase. Under the effect of the two kinds of stress, the face shell breaks. The sudden release of gas would push the reaction film into the titanium melt forming surface pores as A and B shown in Fig. 11a.

The experimental results can be explained based on this model. The addition of starch increases the closed porosity greatly no matter where it is added, which promotes the release of residue gas. As for fiber addition samples (F1, F2 and F3), things are quite different. The pores in F1 and F3 samples are mainly open pores because of the airway formed by nylon fiber after sintering, while for F2 sample, fiber is added to the back layer with a dense primary layer, and the closed porosity is relatively large. As a result, the samples contain more closed pores (S1, S2, S3 and F2), leading to a fluctuant metal surface with obvious pores as Fig. 4a–c, e shows. As for samples F1 and F3 which contain more open pores, the amount of residue gas in the shell mold is not as large. Gas release in these samples is not violent and only happens occasionally, leading to a much flatter metal surface, as shown in Fig. 5d, f. At the same time, the broken region is not as compact as before, which promotes the chemical scab at the surface of metal, as shown in Figs. 5 and 6.

Then, it comes to the third stage; if the melt has severe surface turbulence, the surface pore would be entrained and folded in the melt forming internal pores as A and A<sub>1</sub>

shown in Fig. 11. If the melt flows mildly, the surface pores would stay there till solidification as B and B<sub>1</sub> shown in Fig. 11. In this stage, the flow condition of the melt is the key factor. According to Campbell's theory [27], Weber number ( $We$ ) instead of Reynolds number ( $Ra$ ) should be the variate to characterize whether film at the melt surface could be entrained in because what  $Ra$  represents was internal turbulent, while what  $We$  represents was surface turbulent.  $We$  can be calculated as Eq. (3) shows.

$$We = \frac{\rho V^2 L}{\sigma} \quad (3)$$

where  $\rho$  is fluid density;  $V$  is fluid velocity;  $L$  is characteristic length;  $\sigma$  is coefficient of surface tension.

According to Owen et al.'s [28] and Baghani et al.'s [29] studies,  $We = 1$  was the demarcation point between surface turbulence and surface laminar flow in casting production. When  $We$  is much larger than 1, meaning that inertia force is much larger than surface tension, the surface flow will have severe turbulence. The surface pores would be entrained inside the melt at this time, forming the internal pores shown in Figs. 4e and 5. When  $We$  is less than 1, meaning that surface tension dominates the flow type, the surface pore would stay there, as shown in Figs. 4a–c, e and 5.

However, it is not over. As titanium films are dissolvable in titanium melt according to Hu et al.'s study [30]. Some entrained films in the deep of the melt can re-melt if the temperature is high enough. As a result, hot isostatic pressing (HIP) is often applied to eliminate these entrained film defects. However, the melt near the surface is solidified quickly and some inclusions might be wrapped by the films. In these situations, the entrained films could not re-melt and remain as defects as the long tail and inclusions shown in Figs. 6 and 4e. The long tail shown in Fig. 6 is entrained film which is not completely dissolved.

## 4 Conclusion

The interface reaction layer between Ti–6Al–4V and Y<sub>2</sub>O<sub>3</sub>–silica sol shell mold is very thin in this experiment. Y<sub>2</sub>O<sub>3</sub>–silica sol system is a qualified primary layer system to cast Ti–6Al–4V. The increase in porosity of shell mold does not have remarkable influence on the direct chemical reaction.

The Y<sub>2</sub>O<sub>3</sub>–silica sol primary shell contains more than 1 vol% closed porosity, and Al–Si back shell contains more than 3 vol% closed porosity. The residue gas in the closed pore cannot be expelled even under vacuum.

The surface defects forming process can be divided into three stages: the direct chemical reaction stage, the residue



gas release stage and the entraining stage. An increase in closed porosity intensifies the release of residue gas, while the increase in apparent porosity makes nearly no difference on the interface reaction.

**Acknowledgements** This study was financially supported by the National Natural Science Foundation of China (No. 50875144).

## References

- [1] Saha RL, Jacob KT. Casting of titanium and its alloys. *Def Sci J*. 2014;36(2):121.
- [2] Nastac L, Gungor MN, Klug KL, Tack WT. Advances in investment casting of Ti–6Al–4V alloy: a review. *Int J Cast Met Res*. 2006;19(2):73.
- [3] Sung SY, Kim YJ. Alpha-case formation mechanism on titanium investment castings. *Mater Sci Eng, A*. 2005;405(1):173.
- [4] Kumar S, Narayanan TNS, Raman SGS, Seshadri SK. Thermal oxidation of Ti6Al4V alloy: microstructural and electrochemical characterization. *Mater Chem Phys*. 2010;119(1–2):345.
- [5] Liu AH. The interfacial reaction law and micromechanism between titanium alloy melts and ceramic mould. Harbin: Harbin Institute of Technology; 2007. 30.
- [6] Cotton JD, Clark LP, Phelps HR. Titanium investment casting defects: a metallographic overview. *JOM*. 2006;58(6):13.
- [7] Boettinger W, Williams J, Coriell M, Kattner E, Mueller S. Alpha case thickness modeling in investment castings. *Metall Mater Trans B*. 2000;31(6):1419.
- [8] Lin KF, Lin CC. Interfacial reactions between zirconia and titanium. *Scr Mater*. 1998;39(10):1333.
- [9] Kim MG, Kim SK, Kim YJ. Effect of mold material and binder on metal-mold interfacial reaction for investment casting of titanium alloys. *Mater Trans*. 2002;43(4):745.
- [10] Jerry CL, Anthony JF, Eoin JB. Inert calcia facecoats for investment casting of titanium and titanium–aluminide alloys. US Patent; 5766329.1998.
- [11] Cheng X, Sun XD, Yuan C, Green NR, Withey PA. An investigation of a TiAlO based refractory slurry face coat system for the investment casting of Ti–Al alloys. *Intermetallics*. 2012;29:61.
- [12] Peng XM, Wu AR, Dong LJ, Tao YR, Gao WG, Zhou XL. Stability of NiCrAlY coating/titanium alloy system under pure thermal exposure. *Rare Met*. 2017;36(8):659.
- [13] Neto RL, Duarte TP, Alves JL, Barrigana TG, Da SL. The influence of face coat material on reactivity and fluidity of the Ti6Al4V and TiAl alloys during investment casting. *Proc Inst Mech Eng, Part L*. 2017;231(1-2):38.
- [14] Holcombe CE, Serandos TR. Consideration of yttria for vacuum induction melting of titanium. *Metall Trans B Process Metall*. 1983;14(3):497.
- [15] Gao M, Cui RJ, Ma LM, Zhang HR, Tang XX, Zhang H. Physical erosion of yttria crucibles in Ti–54Al alloy casting process. *J Mater Process Technol*. 2011;211(12):2004.
- [16] Lapin J, Gabalcova Z, Pelachova T. Effect of Y<sub>2</sub>O<sub>3</sub> crucible on contamination of directionally solidified intermetallic Ti–46Al–8Nb alloy. *Intermetallics*. 2011;19(3):401.
- [17] Tetsui T, Kobayashi T, Ueno T, Harada H. Consideration of the influence of contamination from oxide crucibles on TiAl cast material, and the possibility of achieving low-purity TiAl precision cast turbine wheels. *Intermetallics*. 2012;31:274.
- [18] Zhao ET, Kong FT, Chen YY. Effect of different primary coating materials and mold temperatures on fluidity of high-temperature titanium alloy. *Proc Inst Mech Eng, B J Eng Manuf*. 2012;226(11):1862.
- [19] Wei YM, Hu KH, Lu ZG. Effect of SiO<sub>2</sub> concentration in silica sol on interface reaction during titanium alloy investment casting. *China Foundry*. 2018;15(1):23.
- [20] Kostov A, Friedrich B. Predicting thermodynamic stability of crucible oxides in molten titanium and titanium alloys. *Comp Mater Sci*. 2006;38(2):374.
- [21] Wei YM, Lu ZG, Wu GP, Long XQ. Reaction between Ti–6Al–4V and Y<sub>2</sub>O<sub>3</sub>–SiO<sub>2</sub> based face shell for investment casting. *Rare Met*. 2016;35(12):901.
- [22] Cheng X, Yuan C, Blackburn S, Withey PA. The study of the influence of binder systems in an Y<sub>2</sub>O<sub>3</sub>–ZrO<sub>2</sub> face coat material on the investment casting slurries and shells properties. *J Eur Ceram Soc*. 2014;34(12):3061.
- [23] Guo X, Wei YM, Lu ZG. Reaction of titanium investment castings made by Zr (CH<sub>3</sub>COO)<sub>2</sub>–Y<sub>2</sub>O<sub>3</sub> shell. *Rare Met*. 2017; 36(6):465.
- [24] Campbell J. Casting (Second Edition). Li DZ, Li YY, translated. Beijing: Science Press, 2011.16.
- [25] Srivastava D, Chang IT, Loretto MH. The effect of process parameters and heat treatment on the microstructure of direct laser fabricated TiAl alloy samples. *Intermetallics*. 2001;9(12): 1003.
- [26] Malan AG. Investigation into the continuum thermodynamic modelling of investment casting shell-mould drying. Wales Swansea: University of Wales Swansea; 2003. 10.
- [27] Mi J, Harding RA, Wickins M, Campbell J. Entrained oxide films in TiAl castings. *Intermetallics*. 2003;11(4):377.
- [28] Owen EA, Davies DA. An X-ray study of the mutual solid solubilities of zinc and cadmium. *Br J Appl Phys*. 1965;16(9): 1291.
- [29] Baghani A, Bahmani A, Davami P, Varahram N, Shabani MO. Application of computational fluid dynamics to study the effects of sprue base geometry on the surface and internal turbulence in gravity casting. *Proc Inst Mech Eng, L J Mater Des Appl*. 2015; 229(12):106.
- [30] Wu XH, Huang A, Hu D, Loretto MH. Oxidation-induced embrittlement of TiAl alloys. *Intermetallics*. 2009;17(7):540.